Published on 30 April 2014. Downloaded by Hefei Institutes of Physical Science, Chinese Academy of Sciences on 13/10/2014 03:47:56.

Journal of Materials Chemistry A

COMMUNICATION

View Article Online
View Journal | View Issue

Controllable fabrication of dendritic mesoporous silica–carbon nanospheres for anthracene removal†

Cite this: J. Mater. Chem. A, 2014, 2, 11045

Received 28th March 2014
Accepted 30th April 2014

DOI: 10.1039/c4ta01516a

www.rsc.org/MaterialsA

Jianping Yang,‡[ab] Wangyuan Chen,‡[a] Dengke Shen,[b] Yong Wei,[b] Xianqiang Ran,[a] Wei Teng,[a] Jianwei Fan,*[a] Wei-xian Zhang*[a] and Dongyuan Zhao[b]

Dendritic mesoporous silica–carbon nanospheres with a uniform size (~100 nm), high surface area (646 $m^2 g^{-1}$), large pore volume (1.4 $cm^3 g^{-1}$) and center-radial oriented open mesopore channels (7.3 nm) have been fabricated by combining an oil–water biphase stratification and an *in situ* carbonization of surfactant template strategy.

Ordered mesoporous materials with unique physical and chemical properties have attracted great attention in recent years because of their specific controllable mesopore channels for loading and confined effects as well as their widespread applications for drug-delivery carriers, adsorption, catalysis and nanodevices.[1–4] For such applications with unique requirements, a series of mesoporous materials with various frameworks, porosities and compositions, including mesoporous silica, carbon, titanium oxide and metal compounds, have been fabricated.[5–9] Apart from developing the synthesis strategies of various mesoporous materials, significant efforts have been dedicated to exploring facile and effective approaches to construct controllable shapes and sizes with diversified composites and sophisticated architectures.[10–16] Among them, dendritic hierarchical nanospheres present center-radial oriented open and large mesopores, which are more favorable to access and control loading and mass transport. These features render them as nanocontainers and show their great promise for catalysis, adsorption, bioseparation, biolabeling and release.[17–24]

Currently, dendritic mesoporous silica nanospheres are fabricated using an ethyl ether emulsion approach[19] and a facile oil–water biphase stratification strategy.[20] However, it is still difficult to synthesize carbon-based dendritic mesoporous nanospheres with large open mesopores and ordered mesostructures. The key reasons could be that unexpected hydrolysis and interaction make it hard to realize a controlled nucleation and assembly process between precursors and surfactants.[25–27] Particularly, carbon-based dendritic mesoporous nanospheres are highly attractive due to their fascinating and unique properties such as hydrophobic features, chemical inertness, biocompatibility and electrical conductivity. Such properties have been considered to have tremendous potential in electrical chemistry, organic separation and hydrophobic drug delivery.[28–34]

Inspired by the features of cetyltrimethylammonium chloride (CTAC) molecules, which not only can act as a surfactant template to create center-radial oriented open mesopores, but also can be employed as a carbon source *via* the *in situ* carbonization approach in the channels, herein, we introduce a facile and efficient surfactant template carbonization approach to prepare dendritic mesoporous silica–carbon nanospheres with large accessible and hydrophobic mesopore channels for polycyclic aromatic hydrocarbon adsorption.

The successful fabrication of dendritic mesoporous silica–carbon nanospheres is greatly dependent on two aspects. The first one is the synthesis of dendritic mesoporous silica nanospheres, the other one is the coating of the mesopore channels with a carbon layer. The approach is illustrated in Scheme 1, firstly, the dendritic mesoporous silica nanospheres (DMSNs) are synthesized *via* a facile oil–water biphase stratification strategy. Then, the CTAC surfactant of the as-made DMSN products can be treated through three different routes. The products were directly calcined under an air or argon atmosphere to result in the total or partial removal of the CTAC surfactant, denoted as DMSNs-O_2 and DMSNs-Ar, respectively. To improve the carbon content, the as-made DMSNs was pretreated with H_2SO_4 before calcination under an argon atmosphere, leading to the formation of dendritic mesoporous silica–carbon nanospheres (DMSCNs).

The dendritic mesoporous silica nanospheres (DMSNs) are synthesized using an oil–water biphase stratification approach.[20]

[a]College of Environmental Science and Engineering, State Key Laboratory of Pollution Control and Resources Reuse, Tongji University, Shanghai 200092, P. R. China. E-mail: fanjianwei@tongji.edu.cn; zhangwx@tongji.edu.cn

[b]Department of Chemistry, Laboratory of Advanced Materials, Fudan University, Shanghai 200433, P. R. China

† Electronic supplementary information (ESI) available. See DOI: 10.1039/c4ta01516a

‡ These authors contributed equally to this work.

Published on 30 April 2014. Downloaded by Hefei Institutes of Physical Science, Chinese Academy of Sciences on 13/10/2014 03:47:56.

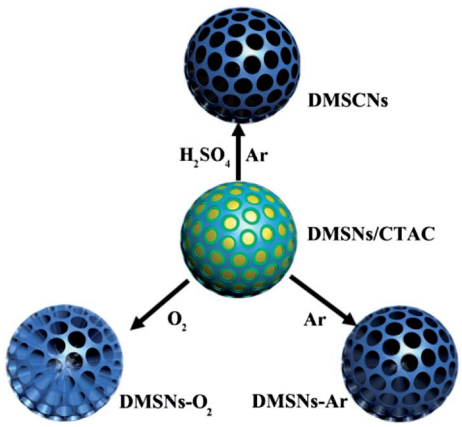

Scheme 1 Schematic representation of the preparation of the dendritic mesoporous silica–carbon nanospheres. The process involves three different post-treatment routes. The dendritic mesoporous silica nanospheres (DMSNs) were directly calcined under an air or argon atmosphere to produce DMSNs-O_2 and DMSNs-Ar, respectively. The DMSN sample was pretreated with H_2SO_4 before calcination under an argon atmosphere, leading to the formation of dendritic mesoporous silica–carbon nanospheres (DMSCNs).

The upper oil phase contains the silica source (tetraethyl orthosilicate, TEOS) and hydrophobic organic solution (cyclohexane), and the lower aqueous phase is the mixture solution of the surfactant (CTAC) and catalyst (triethanolamine, TEA). The field-emission scanning electron microscopy (FESEM) image reveals that the DMSNs have a uniform spherical morphology with a size of ~110 nm (Fig. S1A†). The small-angle X-ray scattering (SAXS) pattern of the DMSNs shows an obvious scattering peak at $q = 0.70\ nm^{-1}$ (Fig. 1A (a)), indicating an ordered mesostructure. It was found that the scattering peak shifted to higher q-values ($0.75, 0.73$ and $0.71\ nm^{-1}$) after the calcination treatment (Fig. 1A (b–d)), suggesting a certain extent of shrinkage. Furthermore, the q-value for the DMSCN samples is observed to be only a little higher, which can be ascribed to the carbon layer in the mesopore channels favorable for preserving the shrinkage of the mesostructure.[9] This phenomenon can also be confirmed by the small-angle X-ray diffraction (XRD) pattern (Fig. S2†). It is worth noting that no morphology change is observed after the calcination treatment (Fig. S1B, C and D†). The DMSNs-O_2, DMSNs-Ar and DMSCNs also present uniform nanospheres with a diameter of ~100 nm and large open pores of ~7 nm on the surface, as shown by the FESEM images (Fig. 1B–D). Transmission electron microscopy (TEM) images clearly show the dendritic pores of center-radial open mesopore channels (Fig. 1B–D, insets). Significantly, these nanospheres are well dispersed and without aggregation after the calcination treatments.

N_2 adsorption–desorption isotherms of the samples DMSNs-O_2, DMSNs-Ar and DMSCNs all display typical type-IV curves with a sharp capillary condensation step in the high relative pressure range of 0.60–0.78, demonstrating the existence of a uniform and large mesopore size (Fig. 2A). The pore size distribution curves, calculated using the Barrett–Joyner–Halenda (BJH) model derived from the adsorption branch, show an intense and narrow mesopore centered around 7 nm (Fig. 2B). Furthermore, the samples DMSNs-O_2, DMSNs-Ar and DMSCNs possess high surface areas (585, 640 and 646 $m^2\ g^{-1}$, respectively) and large pore volumes (1.2, 1.3 and 1.4 $cm^3\ g^{-1}$, respectively) (Table S2†).

It should be mentioned that the CTAC surfactant molecules were completely removed around 600 °C under an air atmosphere, as confirmed by the thermogravimetric analysis (TGA) curves (Fig. S3†) and the disappearance of the absorption bands

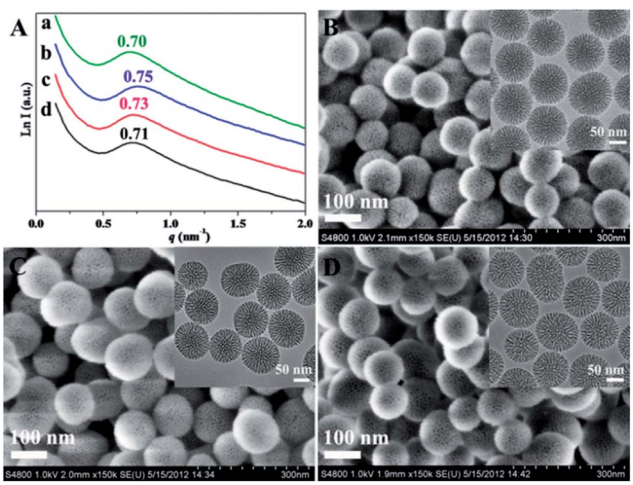

Fig. 1 (A) SAXS patterns of the (a) as-made dendritic mesoporous silica nanosphere (DMSN) sample prepared using an oil–water biphase stratification approach, (b) DMSNs-O_2 (calcined under an air atmosphere), (c) DMSNs-Ar (calcined under an argon atmosphere) and (d) DMSCNs (pretreated with H_2SO_4 before calcination under an argon atmosphere). FESEM and TEM images of (B) DMSNs-O_2, (C) DMSNs-Ar and (D) DMSCNs.

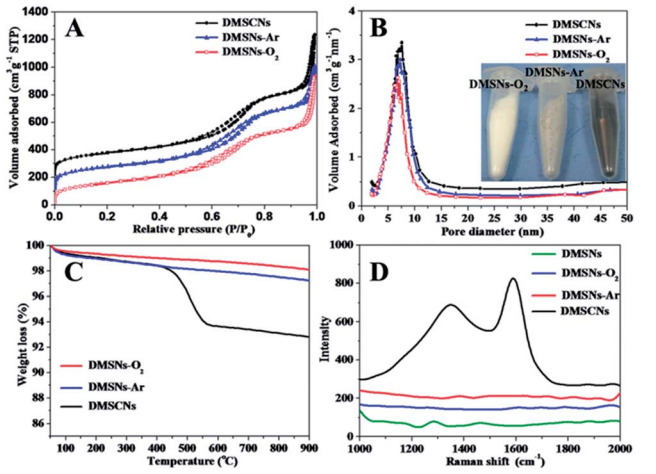

Fig. 2 (A) Nitrogen sorption isotherm curves, (B) pore size distribution plots (the inset is a photograph of the products with different colors), (C) TGA curves under an air atmosphere and (D) Raman spectra of the as-made dendritic mesoporous silica nanosphere (DMSN) sample prepared using an oil–water biphase stratification approach, DMSNs-O_2 (calcined under an air atmosphere), DMSNs-Ar (calcined under an argon atmosphere) and DMSCNs (pretreated with H_2SO_4 before calcination under an argon atmosphere).

 This journal is © The Royal Society of Chemistry 2014

Published on 30 April 2014. Downloaded by Hefei Institutes of Physical Science, Chinese Academy of Sciences on 13/10/2014 03:47:56.

around 2920 and 2849 cm^{-1} for the C–H bonds in the Fourier transform infra-red (FTIR) spectra (Fig. S4†). However, the CTAC molecules were partly carbonated under an argon atmosphere and located into the mesopore channels with a carbon content of about 1 wt% (Fig. 2C, DMSNs-Ar). Additionally, the DMSNs-Ar changed from white to gray in color, suggesting the existence of some carbon residuals in the channels (Fig. 2B, inset). To further prevent the degradation of CTAC, a pretreatment process was adopted for the as-made DMSN sample using H_2SO_4 carbonization before calcination under an argon atmosphere. The carbon content can be successfully improved to 6 wt% for the DMSCN sample (Fig. 2C, DMSCNs). When combined with elemental mapping of Si, O and C (Fig. S5†) and the TEM image before (Fig. 1D) and after etching of the silica framework (Fig. S6†), these results indicate that most of the CTAC converted into tiny carbon nanoparticle species and homogeneously dispersed in the mesoporous channels to form the dendritic mesoporous silica–carbon nanospheres. It is noteworthy that the weight loss plateau shifted to 550 °C under an air atmosphere for DMSCNs, associated with the decomposition of the carbon species (Fig. 2C, DMSCNs). Significantly, the obtained DMSCNs are black in color and are well dispersed in water (Fig. S7†). Moreover, the degree of graphitization for the carbon species was evaluated by the Raman spectra, two strong and obvious D (1350 cm^{-1}) and G (1590 cm^{-1}) bands appear, which correspond to the breathing mode of the aromatic rings and the bond stretching of the sp^2 carbon, respectively (Fig. 2D, DMSCNs). This result is consistent with the presence of disordered sp^2 C atoms in the condensed aromatic carbon with a low degree of graphitization. The characterization of the amorphous carbon is in good agreement with the XRD patterns (Fig. S8†). Thus, the dendritic mesoporous silica–carbon nanospheres with a unique shape, large pore size and pore volume, combined with a high aromatic carbon content deposited on the mesopore channels, are highly promising for adsorption.

Polycyclic aromatic hydrocarbons (PAHs) are among the most frequently detected environmental pollutants due to their persistence in the environment, bioaccumulation, mutagenic, carcinogenic and toxic properties.[35] Moreover, PAHs are highly hydrophobic organic compounds, which have a low biodegradability due to their complex molecular structures and chemical stability.[36] So far, adsorption and enrichment are the most cost-effective treatment techniques due to the operational simplicity, low cost and insensitivity to organic pollutants.[37–39] Therefore, it is highly desirable to develop more efficient and green adsorbents with fast adsorption kinetics and high adsorption capacity for the removal of PAHs.[37] Herein, anthracene was selected as a model PAH to investigate the adsorption chemistry. The adsorption isotherms of DMSNs-O_2, DMSNs-Ar and DMSCNs for anthracene in a cyclohexane solution were determined, as shown in Fig. 3A. It was found that the DMSNs-Ar displayed a similar adsorption behavior as the DMSNs-O_2, which was ascribed to the analogous physicochemical properties and low carbon content (1 wt%). Interestingly, DMSCNs had the highest adsorption capacity among the samples, especially under high concentration conditions. At a concentration of

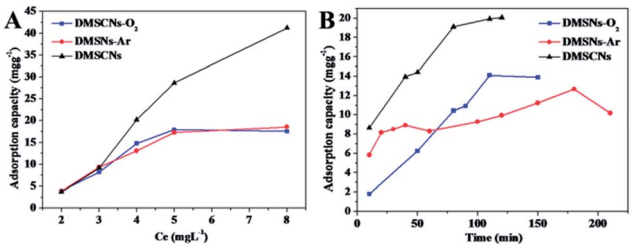

Fig. 3 (A) Adsorption isotherms and (B) adsorption kinetics of DMSNs-O_2 (calcined under an air atmosphere), DMSNs-Ar (calcined under an argon atmosphere) and DMSCNs (pretreated with H_2SO_4 before calcination under an argon atmosphere) in cyclohexane for anthracene.

8 mg L^{-1}, the adsorption capacity of DMSNs-O_2, DMSNs-Ar and DMSCNs is 17.53, 18.55 and 41.19 mg g^{-1}, respectively. Another interesting phenomenon is that DMSCNs exhibit rapid adsorption rates, reaching an equilibrium within 2 h with a saturated capacity of 20.22 mg g^{-1} in the case of a relatively low concentration of anthracene (4 mg L^{-1}) in the cyclohexane solution (Fig. 3B). The remarkable anthracene capture performance showing a high adsorption capacity and fast kinetic equilibrium originates directly from the novel dendritic mesoporous silica–carbon nanospheres which combine a number of unique features. The high surface area, large pore size and open pore network facilitate the efficient accessibility for anthracene. In addition, the uniform shapes with small diameters, dendritic-like architectures and short mesopore channels promote the fast molecular diffusion (Fig. S9†). Simultaneously, the high aromatic carbon matrix deposited on the mesopore channels provides discrete adsorption active sites for the anthracene capture, as well as the high capacity due to the hydrophobic interaction.

Conclusions

In summary, dendritic mesoporous silica–carbon nanospheres with unique nanoarchitectures and excellent adsorption performance for anthracene have been designed and fabricated, combining an oil–water biphase stratification approach and an *in situ* carbonization of surfactant template strategy. This synthesis process is accomplished by a facile oil–water biphase stratification route with TEOS in cyclohexane as the oil phase and TEA in a CTAC surfactant aqueous solution as the water phase to create dendritic mesoporous silica nanospheres. Different calcination steps result in the total and partial removal of the CTAC surfactant to produce DMSNs-O_2 and DMSNs-Ar. Upon a pre-treatment process using H_2SO_4 carbonization before calcination under an argon atmosphere, the CTAC surfactant molecules can be converted into a carbon matrix *in situ* and deposited on the mesopore channels to form DMSCNs. This step is crucial to promote the carbonization. Utilizing those techniques, DMSNs-O_2, DMSNs-Ar and DMSCNs can be selectively produced with high surface areas (585, 640 and 646 m^2 g^{-1}), large pore volumes (1.2, 1.3 and 1.4 cm^3 g^{-1}), open pore sizes (6.7, 7.2 and 7.3 nm) and different carbon

Published on 30 April 2014. Downloaded by Hefei Institutes of Physical Science, Chinese Academy of Sciences on 13/10/2014 03:47:56.

contents (0, 1 and 6 wt%), respectively. Furthermore, the DMSCNs show an excellent adsorption performance and rapid kinetic equilibrium for anthracene removal. Moreover, the DMSCNs offer potential applications in drug delivery, adsorption, loading and catalysis.

Acknowledgements

We gratefully acknowledge the fund supported by the NSFC Grant 21277102, Science and Technology Commission of Shanghai (Grant 11JC1412600) and China Postdoctoral Science Foundation (2014M551455 and 2013M531113). We acknowledge the financial supports of the State Key Laboratory of Pollution Control and Resource Reuse Foundation (PCRRF12001), the National Key Technology R&D Program (2012BAJ25B07), the National Natural Science Foundation of China (21377096), the economic and information committee cooperation plan of Shanghai (04002530571) and the science and technology committee plan of Shanghai Qingpu district (04002370168).

Notes and references

1 Y. Wan and D. Y. Zhao, *Chem. Rev.*, 2007, **107**, 2821–2860.
2 M. Hartmann, *Chem. Mater.*, 2005, **17**, 4577–4593.
3 C.-H. Lee, T.-S. Lin and C.-Y. Mou, *Nano Today*, 2009, **4**, 165–179.
4 A. Taguchi and F. Schüth, *Microporous Mesoporous Mater.*, 2005, **77**, 1–45.
5 K. Ariga, A. Vinu, Y. Yamauchi, Q. Ji and J. P. Hill, *Bull. Chem. Soc. Jpn.*, 2012, **85**, 1–32.
6 Y. Meng, D. Gu, F. Q. Zhang, Y. F. Shi, H. F. Yang, Z. Li, C. Z. Yu, B. Tu and D. Y. Zhao, *Angew. Chem.*, 2005, **117**, 7215–7221.
7 P. D. Yang, D. Y. Zhao, D. I. Margolese, B. F. Chmelka and G. D. Stucky, *Nature*, 1998, **396**, 152–155.
8 W. Luo, Y. H. Li, J. P. Dong, J. Wei, J. Q. Xu, Y. H. Deng and D. Y. Zhao, *Angew. Chem., Int. Ed.*, 2013, **52**, 10505–10510.
9 J. Lee, M. C. Orilall, S. C. Warren, M. Kamperman, F. J. DiSalvo and U. Wiesner, *Nat. Mater.*, 2008, **7**, 222–228.
10 D. Y. Zhao, J. Y. Sun, Q. Z. Li and G. D. Stucky, *Chem. Mater.*, 2000, **12**, 275–279.
11 H.-P. Lin and C.-Y. Mou, *Acc. Chem. Res.*, 2002, **35**, 927–935.
12 C. Z. Yu, J. Fan, B. Z. Tian and D. Y. Zhao, *Chem. Mater.*, 2004, **16**, 889–898.
13 W. C. Yoo and A. Stein, *Chem. Mater.*, 2011, **23**, 1761–1767.
14 J. Liu, S. Z. Qiao, J. S. Chen, X. W. D. Lou, X. Xing and G. Q. M. Lu, *Chem. Commun.*, 2011, **47**, 12578–12591.
15 B. G. Trewyn, C. M. Whitman and V. S. Y. Lin, *Nano Lett.*, 2004, **4**, 2139–2143.
16 J. Kobler, K. Möller and T. Bein, *ACS Nano*, 2008, **2**, 791–799.
17 V. Polshettiwar, D. Cha, X. Zhang and J. M. Basset, *Angew. Chem., Int. Ed.*, 2010, **49**, 9652–9656.
18 M.-H. Kim, H.-K. Na, Y.-K. Kim, S.-R. Ryoo, H. S. Cho, K. E. Lee, H. Jeon, R. Ryoo and D.-H. Min, *ACS Nano*, 2011, **5**, 3568–3576.
19 X. Du, B. Shi, J. Liang, J. Bi, S. Dai and S. Z. Qiao, *Adv. Mater.*, 2013, **25**, 5981–5985.
20 D. K. Shen, J. P. Yang, X. M. Li, L. Zhou, R. Y. Zhang, W. Li, L. Chen, R. Wang, F. Zhang and D. Y. Zhao, *Nano Lett.*, 2014, **14**, 923–932.
21 K. Zhang, L.-L. Xu, J.-G. Jiang, N. Calin, K.-F. Lam, S.-J. Zhang, H.-H. Wu, G.-D. Wu, B. Albela, L. Bonneviot and P. Wu, *J. Am. Chem. Soc.*, 2013, **135**, 2427–2430.
22 J. P. Yang, Y. H. Deng, Q. L. Wu, J. Zhou, H. F. Bao, Q. Li, F. Zhang, F. Y. Li, B. Tu and D. Y. Zhao, *Langmuir*, 2010, **26**, 8850–8856.
23 J. P. Yang, F. Zhang, Y. R. Chen, S. Qian, P. Hu, W. Li, Y. H. Deng, Y. Fang, L. Han, M. Luqman and D. Y. Zhao, *Chem. Commun.*, 2011, **47**, 11618–11620.
24 J. P. Yang, D. K. Shen, L. Zhou, W. Li, X. M. Li, C. Yao, R. Wang, A. M. El-Toni, F. Zhang and D. Y. Zhao, *Chem. Mater.*, 2013, **25**, 3030–3037.
25 Y. Fang, D. Gu, Y. Zou, Z. X. Wu, F. Y. Li, R. C. Che, Y. H. Deng, B. Tu and D. Y. Zhao, *Angew. Chem., Int. Ed.*, 2010, **49**, 7987–7991.
26 J. Liu, T. Y. Yang, D.-W. Wang, G. Q. Lu, D. Y. Zhao and S. Z. Qiao, *Nat. Commun.*, 2013, **4**, 2798–2804.
27 D. Gu, H. Bongard, Y. H. Deng, D. Feng, Z. X. Wu, Y. Fang, J. J. Mao, B. Tu, F. Schüth and D. Y. Zhao, *Adv. Mater.*, 2010, **22**, 833–837.
28 H. Q. Qin, Z. Y. Hu, F. J. Wang, Y. Zhang, L. Zhao, G. J. Xu, R. A. Wu and H. F. Zou, *Chem. Commun.*, 2013, **49**, 5162–5164.
29 Q. Yue, M. H. Wang, J. Wei, Y. H. Deng, T. Y. Liu, R. C. Che, B. Tu and D. Y. Zhao, *Angew. Chem., Int. Ed.*, 2012, **51**, 10368–10372.
30 J. Schuster, G. He, B. Mandlmeier, T. Yim, K. T. Lee, T. Bein and L. F. Nazar, *Angew. Chem., Int. Ed.*, 2012, **51**, 3591–3595.
31 T. Y. Yang, J. Liu, Y. Zheng, M. J. Monteiro and S. Z. Qiao, *Chem. –Eur. J.*, 2013, **19**, 6942–6945.
32 Y. P. Zhai, Y. Q. Dou, D. Y. Zhao, P. F. Fulvio, R. T. Mayes and S. Dai, *Adv. Mater.*, 2011, **23**, 4828–4850.
33 J. P. Yang, D. K. Shen, L. Zhou, W. Li, J. W. Fan, A. M. El-Toni, W.-X. Zhang, F. Zhang and D. Y. Zhao, *Adv. Healthcare Mater.*, 2014, DOI: 10.1002/adhm.201400053.
34 J. P. Yang, F. Zhang, W. Li, D. Gu, D. K. Shen, J. W. Fan, W.-X. Zhang and D. Y. Zhao, *Chem. Commun.*, 2014, **50**, 713–715.
35 J. Josephson, *Environ. Sci. Technol.*, 1984, **18**, 93A–95A.
36 W. N. Wang, R. Y. Ma, Q. H. Wu, C. Wang and Z. Wang, *J. Chromatogr. A*, 2013, **1293**, 20–27.
37 K. Yang, L. Z. Zhu and B. S. Xing, *Environ. Sci. Technol.*, 2006, **40**, 1855–1861.
38 X.-B. Zhang, H.-W. Tong, S.-M. Liu, G.-P. Yong and Y.-F. Guan, *J. Mater. Chem. A*, 2013, **1**, 7488–7493.
39 T. Hüffer, M. Kah, T. Hofmann and T. C. Schmidt, *Environ. Sci. Technol.*, 2013, **47**, 6935–6942.

 This journal is © The Royal Society of Chemistry 2014